HHS Public Access

Author manuscript

Toxicol Appl Pharmacol. Author manuscript; available in PMC 2020 December 15.

Published in final edited form as:

Toxicol Appl Pharmacol. 2020 March 01; 390: 114898. doi:10.1016/j.taap.2020.114898.

Comparative analysis of lung and blood transcriptomes in mice exposed to multi-walled carbon nanotubes

Timur O. Khaliullin[a,b,1], **Naveena Yanamala**[b,1], **Mackenzie S. Newman**[a], **Elena R. Kisin**[b], **Liliya M. Fatkhutdinova**[c], **Anna A. Shvedova**[a,b,*]

[a]Department of Physiology and Pharmacology, West Virginia University, Morgantown, WV, USA

[b]Health Effects Laboratory Division, NIOSH, CDC, Morgantown, WV, USA

[c]Department of Hygiene and Occupational Medicine, Kazan State Medical University, Kazan, Russia

Abstract

Pulmonary exposure to multi-walled carbon nanotubes (MWCNT) causes inflammation, fibroproliferation, immunotoxicity, and systemic responses in rodents. However, the search for representative biomarkers of exposure is an ongoing endeavor. Whole blood gene expression profiling is a promising new approach for the identification of novel disease biomarkers. We asked if the whole blood transcriptome reflects pathology-specific changes in lung gene expression caused by MWCNT. To answer this question, we performed mRNA sequencing analysis of the whole blood and lung in mice administered MWCNT or vehicle solution via pharyngeal aspiration and sacrificed 56 days later. The pattern of lung mRNA expression as determined using Ingenuity Pathway Analysis (IPA) was indicative of continued inflammation, immune cell trafficking, phagocytosis, and adaptive immune responses. Simultaneously, innate immunity-related transcripts (*Plunc*, *Bpifb1, Reg3g*) and cancer-related pathways were downregulated. IPA analysis of the differentially expressed genes in the whole blood suggested increased hematopoiesis,

*Corresponding author at: Health Effects Laboratory Division, NIOSH, CDC, Morgantown, WV, USA. ats1@cdc.gov (A.A. Shvedova).

[1]These authors contributed equally.

Authors' contributions

TK, NY, LF and AS conceptualized the project; TK and EK handled animals, including pharyngeal aspiration and sample collection; TK, MN, NY and EK analyzed and processed results; TK, NY, MN, EK, LF, and AS contributed to the writing and editing of the manuscript. All authors read and approved the final manuscript.

Ethical approval

All experimental procedures were conducted in accordance with the Guide for the Care and Use of Laboratory Animals and approved by the National Institute for Occupational Safety and Health Institutional Animal Care and Use Committee.

Availability of supporting data

All data generated or analyzed during this study that is not included in this published article or its Supplementary materials is available from the corresponding author on reasonable request. Gene expression data is available in the NCBI's Gene Expression Omnibus, accessible via accession number GSE140676.

Disclaimer

The authors alone are responsible for the content of this manuscript. The findings and conclusions in this manuscript are those of the authors and do not necessarily represent the official position of the National Institute for Occupational Safety and Health, Centers for Disease Control and Prevention.

Declaration of Competing Interest

The authors declare that they have no competing interests.

Appendix A. Supplementary data

Supplementary data to this article can be found online at https://doi.org/10.1016/j.taap.2020.114898.

predicted activation of cancer/tumor development pathways, and atopy. There were several common upregulated genes between whole blood and lungs, important for adaptive immune responses: *Cxcr1*, *Cd72*, *Sharpin*, and *Slc11a1*. *Trim24*, important for T_H2 cell effector function, was down-regulated in both datasets. *Hla-dqa1* mRNA was upregulated in the lungs and downregulated in the blood, as was *Lilrb4*, which controls the reactivity of immune response. "Cancer" disease category had opposing activation status in the two datasets, while the only commonality was "Hypersensitivity". Transcriptome changes occurring in the lungs did not produce a completely replicable pattern in whole blood; however, specific systemic responses may be shared between transcriptomic profiles.

Keywords

MWCNT; Whole Blood Transcriptome; Lung Transcriptome; IPA Analysis

1. Introduction

Multi-walled carbon nanotubes (MWCNT) continue to be one of the most auspicious carbonaceous nanomaterials with a plethora of applications. At the same time, there is a continuous push for their toxicological profiling and adopting regulatory guidelines worldwide. From a significant number of toxicological studies, we now understand that upon pulmonary exposure, MWCNT cause local inflammation, fibroproliferative responses, immunotoxicity, and systemic responses (Muller et al., 2005; Shvedova et al., 2005; Lam et al., 2006; Porter et al., 2010; Poulsen et al., 2015). One of the MWCNT varieties (Mitsui-7) is even recognized by International Agency for Research on Cancer as a possible carcinogen for humans (Grosse et al., 2014). We are now at the stage when cohort epidemiological studies are being conducted in workers occupationally exposed to MWCNT, revealing subtle differences in cytokine levels (Fatkhutdinova et al., 2016a; Beard et al., 2018), cardiovascular and lung function (Kuijpers et al., 2018; Schubauer-Berigan et al., 2018), gene expression (Shvedova et al., 2016a), and epigenetic alterations (Ghosh et al., 2017). Despite progress in our understanding of potential hazard and risk assessment, there are still major challenges that haven't been addressed in full, such as the issue of tremendous variety of carbon nanotubes species and the absence of reliable biomarkers of exposure and effect. Current research efforts towards biomarkers, including approaches to biomonitoring in workers are extensively reviewed elsewhere (Iavicoli et al., 2016; Schulte et al., 2018).

One of the promising approaches to biomarkers identification that steadily gains attractiveness is the gene expression profiling of the whole blood or peripheral blood mononuclear cells (PBMC) (Burczynski and Dorner, 2006; Mohr and Liew, 2007). Peripheral blood cells express large amounts of tissue-specific genes, and blood transcripts are responsive to environmental stimuli. (Liew et al., 2006; Winckelmans et al., 2017). During the PBMC isolation procedure some of the transcripts can be lost, whilst whole blood gene expression analysis captures the entire transcriptome. Whole blood gene expression analyses are used in mouse models (Petrov et al., 2016). The fact that the mice are inbred means that individual differences are minimized, which is a big issue in human studies (Whitney et al., 2003). So far, several research groups produced significant amounts

of data on lung transcriptome alterations following exposure to different types of MWCNT (Poulsen et al., 2015; Dymacek et al., 2015; Pacurari et al., 2011; Snyder-Talkington et al., 2016a; Snyder-Talkington et al., 2013), which expanded our understanding of the underlying biological mechanisms, but only one study included the assessment of blood transcriptome in mice exposed to MWCNT (Snyder-Talkington et al., 2016a). All of the studies, however, employed generic commercially-available nanoparticles.

In order to understand the interspecies differences and correlate the obtained results, it is crucial that the MWCNTs in question are the same in both treated animals and realistically exposed human populations. A recent study by our group has shown that in humans it is possible to track dysregulated blood RNA expression between exposed/unexposed cohorts (Shvedova et al., 2016a). It is unknown, though, whether this data can serve as a surrogate for lung tissue gene expression, since obtaining the lung tissue is a much more invasive procedure than blood sampling.

In the current study we attempted to answer the question, whether the whole blood transcriptome reflects changes in lung tissue gene expression profile after pulmonary exposure to MWCNT in mice. We utilized the same material that human workers were/are exposed to at a manufacturing facility (Shvedova et al., 2016a). In addition to histopathological evaluation of lung tissue sections, we compared the mRNA expression profiles of both the lung tissue and the whole blood in a murine model of MWCNT pharyngeal aspiration.

2. Materials and methods

2.1. MWCNT characterization and preparation

MWCNTs were produced by Nanotechcenter Ltd. (Tambov, Russia) by catalytic vapor deposition. According to the provided technical documentation, individual MWCNTs had an outer diameter of 8–15 nm, inner diameter of 4–8 nm, and length 2–15 μm. Total amount of metal catalyst impurities did not exceed 5% and specific geometrical surface was 300–320 m^2/g. MWCNT samples were received as solid samples and sterilized by autoclaving, suspended in sterile Ca^{2+} and Mg^{2+}-free phosphate buffered saline (PBS) at 10 mg/ml concentration, dispersed by brief sonication (30 s) with a probe sonicator (Vibra Cell Sonics, 130 W, 20 kHz, 65% amplitude) and sterilized by autoclaving. Endotoxin levels were measured in sterilized solutions using Limulus amebocyte lysate (LAL) chromogenic endpoint assay kit (Hycult Biotech, Inc., Plymouth Meeting, PA). Endotoxin levels in all samples were below the detection limit (0.01 EU/ml). MWCNT vehicle solutions for animal exposure (1 mg/ml) were prepared from 10 mg/ml autoclaved stock solutions in sterile PBS with the addition of 150 μg/ml of Survanta® (Abbott Laboratories, Columbus, OH) – a natural lung surfactant – as a dispersant, utilized previously for CNT toxicity studies (Wang et al., 2010). MWCNT in vehicle solution were present as individual nanotubes and agglomerates with the size of up to 5 μm (Fig. 1, Supplementary fig. 1) as shown by field emission scanning electron microscope (FESEM, model S-4800; Hitachi, Tokyo, Japan). The intensity weighted particle size distributions in the vehicle solution based on dynamic light scattering (DLS) were determined using a Zetasizer Nano ZS (Malvern Instr., UK) (Supplementary table 1). DLS revealed several peaks between 0.1 and 5 μm, which is in

agreement with the FESEM and the previously reported agglomerate sizes present in the workplace air (Fatkhutdinova et al., 2016b). (See Fig. 1.)

2.2. Animals

Experiments were conducted with adult female C57BL/6 mice (n = 10 per group for a total of 20) (Jackson Laboratories, Bar Harbor, ME), aged 7–8 weeks and weighing 20.2 ± 1.7 g at use. The animals were maintained in individual cages, receiving HEPA-filtered air, and supplied with nutritionally adequate pelleted food (certified feed 7913, Harlan Teklad, Indianapolis, IN) and water ad libitum. Beta Chips (Northeastern Products Corp., Warrensburg, NY) were utilized for bedding and changed weekly. Animals were acclimated in the animal facility for at least one week before MWCNT exposure. All animals were housed in the AAALAC International-accredited National Institute for Occupational and Safety Health (NIOSH) animal facility. All experimental procedures were conducted in accordance with guidelines and policy set forth by the Institute of Laboratory Animal Resources, National Research Council and approved by the CDC-Morgantown Institutional Animal Care and Use Committee (IACUC).

2.3. Animal exposure

Mice were anesthetized with an injection of a mixture of 41.65 mg/kg ketamine and 1.65 mg/kg xylazine, subcutaneously, in the abdominal area (Phoenix, St. Joseph, MO). They were then placed on a board in a near-vertical position and the animal's tongue was extended with forceps. A suspension of MWCNT (40 μg/mouse) was placed posterior in the throat and the tongue was held until the suspension was aspirated into the lungs; control mice were administered vehicle solution (PBS + 150 μg/ml of Survanta®). Pharyngeal aspiration provides good distribution and particle deposition in the lungs, including alveolar space, and corresponds to the inhalation studies results (Shvedova et al., 2008a; Castranova et al., 2013). Previous in vivo dose-response and time course studies of MWCNT exposure in mice demonstrated that pulmonary inflammation and damage appeared 1 day post-exposure, peaked 7 days post-exposure, and started to decline, while MWCNT-induced interstitial fibrosis increased at day 28 and progressed through 56 days (Porter et al., 2010; Mercer et al., 2013; Khaliullin et al., 2015). Hence, we chose to sacrifice the animals at 56 days, when the number of affected immune cell subsets in the blood most likely reverts to baseline values (Fig. 2).

2.4. Blood and tissue collection

Mice were euthanized with an overdose of ≥100 mg/kg of pentobarbital, and deep anesthesia was confirmed when the mouse no longer responded to a toe pinch. Whole blood (~ 0.5 ml) was taken from posterior vena cava and dispensed into PAXgene™ Blood RNA Tubes (Qiagen, USA). Following blood collection, mice were exsanguinated by transection of vena cava and abdominal aorta. The sample was gently inverted and frozen at −80 °C within two hours of collection. Ten mice had their lungs perfused through the right ventricle by sterile PBS, removed, and stored in RNAlater solution (Invitrogen, USA) at −80 °C.

2.5. Histopathology

Half of the mice (n = 5 for each group) had their lungs inflated with buffered formalin and embedded in paraffin blocks. Lung tissue sections were stained by H&E and Masson's Trichrome.

2.6. Hematological analysis

Whole blood (200 μL) was collected in heparin-treated test tubes and hematological cell differentials were determined using a ProCyte-Dx Hematology Analyzer (IDEXX Laboratories, Westbrook, ME).

2.7. Lung tissue microarray sample preparation & analysis

Global gene expression for each treatment was determined using high-throughput mRNA microarray analysis following MIAME guidelines (Brazma et al., 2001). Total RNA was isolated from whole lung tissues of control and MWCNT exposed mice 56 days post exposure (n = 5 for each group). The RNA was isolated using TRIzol reagent (Invitrogen, Carlsbad, CA, USA) and purified using RNeasy MiniKits (Qiagen, Mississauga, ON, Canada) as described by the manufacturer. On-column DNase treatment was applied (Qiagen, Mississauga, ON, Canada). Total RNA from each sample was quantified by the NanoDrop ND-1000 and RNA integrity was assessed by standard denaturing agarose gel electrophoresis. All RNA samples showed an absorbance (A260/280) ratio > 2.0. Total RNA of each sample was used for labeling and array hybridization as the following steps: 1) Reverse transcription with Invitrogen Superscript ds-cDNA synthesis kit; 2) ds-cDNA labeling with NimbleGen one-color DNA labeling kit; 3) Array hybridization using the NimbleGen 12x135K microarray followed by washing with the NimbleGen wash buffer kit; 4) Array scanning using the Axon GenePix 4000B microarray scanner (Molecular Devices Corporation). Scanned images (TIFF format) were then imported into NimbleScan software (version 2.5) for grid alignment and expression data analysis. Expression data were normalized through quantile normalization and the Robust Multichip Average (RMA) algorithm included in the NimbleScan software. The Gene level (*_RMA.calls) files generated after normalization were imported into Agilent GeneSpring GX software (version 12.1) for further analysis. Differentially expressed genes with statistical significance between two groups were identified through Volcano Plot filtering (Li, 2012). A genome-wide 10% false discovery rate (FDR) was applied to this analysis. Genes showing expression changes of at least 1.5-fold in either direction compared to their controls and having and FDR ≤0.1 were considered significantly differentially expressed and were considered for further analysis. All gene expression data were uploaded to NCBI's Gene Expression Omnibus and are accessible via accession number GSE140676.

2.8. Whole blood mRNA isolation, labeling, and array hybridization

RNA was extracted from whole blood using the PAXgene™ Blood RNA System Kit following manufacturer's guidelines. Briefly, the samples were removed from −80 °C and incubated at room temperature for 2 h to ensure complete lysis. After that the tubes were centrifuged for 10 min at 5000g, the supernatant decanted and 500 μL of RNase-free water added to the pellet. After washing with RNase-free water, the pellet was dissolved in 350 μl

resuspension buffer and incubated with 300 μl binding buffer and 40 μl proteinase K for 10 min at 55 °C in a shaker-incubator. The lysate was transferred into a PAXgene shredder spin column and centrifuged (18,000 *g* for 3 min). The flow-through fraction was mixed with 350 μl ethanol and transferred to a PAXgene RNA spin column. After washing the column with washing buffer 1, samples were incubated with 10 μl of DNase I for 15 min. The columns were washed with washing buffer and RNA eluted with 40 μl elution buffer. The RNA yield was estimated by measuring absorbance at 260 nm in a NanoDrop ND-1000 spectrophotometer (Thermo Fisher Scientific, Wilmington, DE, USA). RNA purity was calculated from the ratio of absorbance at 260 nm and 280 nm, and RNA integrity was assessed by standard denaturing agarose gel electrophoresis.

Mouse LncRNA Microarray V3.0, designed by ArrayStar Inc., was employed to perform global profiling of mouse protein-coding (~24,881) transcripts. Sample labeling and array hybridization were performed according to the Agilent One-Color Microarray-Based Gene Expression Analysis protocol (Agilent Technology) with minor modifications. Briefly, mRNA was purified from total RNA after removal of rRNA (mRNA-ONLY™ Eukaryotic mRNA Isolation Kit, Epicentre). Then, each sample was amplified and transcribed into fluorescent cRNA along the entire length of the transcripts without 3′ bias utilizing a random priming method. The labeled cRNAs were purified by RNeasy Mini Kit (Qiagen). The concentration and specific activity of the labeled cRNAs (pmol Cy3/μg cRNA) were measured by NanoDrop ND-1000. 1 μg of each labeled cRNA was fragmented by adding 5 μl 10 × Blocking Agent and 1 μl of 25 × Fragmentation Buffer, then heated the mixture at 60 °C for 30 min, finally 25 μl 2 × GE Hybridization buffer was added to dilute the labeled cRNA. 50 μl of hybridization solution was dispensed into the gasket slide and assembled on to the microarray slide. The slides were incubated for 17 h at 65 °C in an Agilent Hybridization Oven. The hybridized arrays were washed, fixed and scanned with using the Agilent DNA Microarray Scanner (part number G2505C). Agilent Feature Extraction software (version 11.0.1.1) was used to analyze acquired array images. Quantile normalization and subsequent data processing were performed with using the GeneSpring GX v11.5.1 software package (Agilent Technologies). The mRNAs showing expression changes of at least 1.2-fold in the blood in MWCNT-exposed group compared to non-exposed controls, having FDR of less than or equal to 0.1 were considered significantly differentially expressed and were considered for further analysis. Hierarchical Clustering was performed using the Agilent GeneSpring GX software (version 12.1). All mRNA expression data were deposited to NCBI's Gene Expression Omnibus and is accessible via accession number GSE140676.

2.9. Gene expression data analysis using IPA

To identify significantly perturbed biological pathways and signaling networks in mice exposed to MWCNTs, we performed Ingenuity Pathway Analysis (IPA, ver. 8.6; Redwood City, CA; www.ingenuity.com) on differentially expressed mRNAs. Tab delimited text files containing gene IDs, expression data, *t*-test *p*-values, and FDR values were uploaded into IPA for conducting a core and comparison analyses. Score rankings for the top molecular/cellular/biological functions, diseases, toxicology functions, and upstream regulators were calculated using IPA-generated negative logarithm p-values i.e., −log10(p-value) and

associated z- and network scores. The estimated Fischer's exact p-values, pathway- and network-activation scores reflect the probability or likelihood of genes occurring in a given pathway/biofunction/disease/network versus others is based on pure chance or not. The sign of the calculated z-score reflects the overall predicted activation state, with z-scores > 2 or smaller than −2 considered significant.

2.10. ImmQuant myeloid cell differentiation assessment

Tab-delimited text files containing gene names and raw expression data for each control and treatment sample were uploaded to the ImmQuant software and immune cell deconvolution was performed using the program algorithm (Frishberg et al., 2016).

2.11. Statistical analysis

Non-IPA related statistical analyses were performed using R statistical package (http://www.r-project.org). All data are presented as the mean ± the standard error of the mean (SEM).

3. Results

3.1. Lung histopathology

At 56 days post-exposure, microscopic sections in the control group revealed normal histology of conductive and respiratory airways. In treatment group all mice (Poulsen et al., 2015) displayed granulomatous lesions, with clusters of dark pigmented particulate matter agglomerates, mostly inside the macrophages, and surrounded by fibrotic tissue. Masson's trichrome staining of the lung sections revealed increased collagen deposition in the treatment group (Fig. 3).

3.2. Hematological analysis

We assessed the blood cellular composition and other the physiological parameters using ProCyte-Dx Hematology Analyzer and found slight decrease in red blood cell count as well as hemoglobin content in the treated group, however no significant differences in immune cell differentials or other parameters were observed (Supplementary table 2).

3.3. Transcriptional response in the lungs and whole blood of mice exposed to MWCNT

Differential gene expression analysis indicated that MWCNT exposure induced extensive alteration in lung and blood gene expression (Fig. 4). There were 4622 genes differentially expressed between control and treatment groups (fold change ≥ ± 1.5, FDR < 0.1). Among these, 2885 were upregulated and 1737 were downregulated. At 56 days post-exposure to MWCNT, 94 mRNA were upregulated and 186 downregulated in the whole blood of mice compared to the untreated group (fold change ≥ ± 1.2, FDR < 0.1). The highest upregulated genes in the mouse blood included *Ptger2*, *Pcdha2*, *Vdr*, *Mtnr1b*, *Rnf183*, while among the most downregulated were *Mcpt8*, *Mbd4*, *Msh2*, *St 3 gal1*, and *Fcer2*. We have investigated the overlaps between dysregulated genes in both datasets. Ten genes were significantly upregulated and nine downregulated in both datasets. However, more genes had opposite regulation status overall, with three genes upregulated in the whole blood, but

downregulated in the lungs, and twenty-four upregulated in the lung tissue and downregulated in the blood (Table 1).

3.4. ImmQuant myeloid cell differentiation assessment using the gene signatures

The immune cell deconvolution using ImmQuant algorithms predicted that the transcriptional changes observed in the lungs were associated with a relative increase in activated macrophages, classical monocytes, alveolar macrophages, mature T-cells and relative decrease in immature/naïve T-cells, dendritic cells and stem cell progenitors (both AM-specific and common myeloid) 56 days after MWCNT exposure (Supplementary fig. 2). The only significant immune cell subset difference in the blood was a minor relative increase in NK T-cells in treated group (Supplementary fig. 3).

3.5. Core analysis of the dysregulated mRNAs in the lungs of mice exposed to MWCNT

In order to determine the overall role of dysregulated genes in biological functions and predicted outcomes, we performed a detailed analysis using IPA. The summary of the findings can be found in the supplementary files. Top perturbed canonical pathways included Oxidative Phosphorylation, Mitochondrial Dysfunction, B Cell Receptor Signaling, IL-6 Signaling, VEGF Signaling, Role of NFAT in Regulation of the Immune Response, and Dendritic Cell Maturation. Analysis of the upstream regulators revealed significant inhibition of several regulators involved in mTOR pathway (RICTOR), B-cell functions (TCF-3), tumor suppression (KMDA5), and predicted activation of both tumor promoters (HMGN5) and suppressors (RB1, TP53). The analysis also predicted a major activation of FOXO1, which is involved in a variety of important functions, such as wound healing, innate and adaptive immunity, and tumor suppression (Wang et al., 2014). Top Diseases and Bio Functions displayed emphasis on immune cell trafficking and interactions, as well as inflammation and injury (Table 2), which is consistent with the ImmQuant deconvolution findings. Although cancer is listed in the top five, a majority of cancer-related disorders actually have a negative z-score, suggesting of decreased activation. Finally, top molecular networks involved included cell replication, development, injury and repair, morphology and immune response.

3.6. Core analysis of dysregulated mRNAs in the blood of mice exposed to MWCNT

The upstream regulator analysis predicted significant inhibition of the KMT2D transcription regulators, TP53 and GATA1, whereas OGA was predicted to be activated. While the top five diseases and disorders listed connective tissue pathology, injury, inflammation and cancer (Table 3), analysis of the murine blood mRNA microarray data revealed two major entries with the highest Z-score, predicted to be activated: “Cancer” and “Atopy/ Hypersensitivity”; at the same time” DNA transcription” had a negative z-score of −1.655 (Supplementary Fig. 4). The top five affected molecule networks were related to cell and tissue development, cancer, and cell replication, and the regulatory network functions predicted the activation of several important regulators, such as NF-kB and p38 MAPK (Supplementary Fig. 5).

3.7. Comparison analysis in IPA

To assess the possible similarities/dissimilarities in gene expression patterns, we performed a dataset comparison analysis in IPA. In the Diseases and Biological Function category, there was only one major common entry – hypersensitivity reaction (Table 4). Cancer-related items were mostly reverse-related in terms of the predicted activation status between the lung and blood datasets. Opposite activation scores were observed for TP53 upstream regulator and several canonical pathways involved in immune activation (Table 4). There were no strict similarities in the molecular/cellular functions. Although not all of the z-scores reached the −2/+2 significance threshold, the values between 1 and 2 (or −1 and −2) still represent the 15/85 percentiles of the gene directionality distribution.

4. Discussion

The most realistic scenario of human exposure route to MWCNT is inhalation. A recent industry-wide study has determined the mean CNT exposure (based on the elemental carbon content) to be 1.00 μg/m^3 for the respirable fraction and 6.22 μg/m^3 for inhalable (Dahm et al., 2018). Respirable fraction EC content in the air of the factory producing MWCNT used in this study reached 6.11 μg/m^3 (Fatkhutdinova et al., 2016b). The 40 μg of MWCNT dose, employed in this study, was found to be occupationally relevant through the extrapolation of rodent in vivo and in vitro assessments to equivalent human exposures (Erdely et al., 2013; Siegrist et al., 2014). The NIOSH Nanotechnology Research Plan for 2018–2025 includes identification of biomarkers of response to engineered nanomaterials; however, the search for the biomarkers of exposure to nanomaterials and effect is daunting, considering the specific characteristics of nanoparticles and their unpredictable properties (Nel et al., 2015). Peripheral blood provides a safer and more convenient alternative to lung biopsy sampling during bronchoscopy or other invasive procedures. The whole blood genome contains a large amount of tissue-specific transcripts (Liew et al., 2006), but whether those transcripts are dysregulated in the same manner as in lung tissue upon pulmonary exposure to MWCNT is not known. Only one study has assessed whole blood gene expression in MWCNT-exposed animals (Snyder-Talkington et al., 2016b), but that study heavily focused on carcinogenic outcomes, using a mouse model prone to cancer, and using a cancer-promoting agent in the animals. Another study from the same group compared concordant gene expression between mouse tissue/blood and pulmonary cell cultures (Snyder-Talkington et al., 2019), yet they did not specifically compare the lung tissue and blood gene expression profiles. The only two mRNAs mentioned with concordant presence in mouse lung tissue, mouse blood, and human pulmonary epithelial cells were SLC7A1 and SLC22A5. Our study is the first to investigate whole blood transcriptome changes in wild-type animals exposed to MWCNT and cross compare those with lung transcriptome changes. This study uniquely positioned us to compare the whole blood gene expression datasets from MWCNT-administered mice and human populations exposed to the same materials in occupational settings (Shvedova et al., 2016b).

Mice were sacrificed 56 days after exposure, and mRNA microarray study was performed to quantify the changes in lung and whole blood gene expression in addition to histopathological evaluation. Histopathology revealed the presence of MWCNT material in

the lung, together with granulomatous lesions, increase in collagen fibers deposition, and accumulation of macrophages. This is in line with many previous in vivo studies reporting inflammatory and fibrotic responses in rodents upon exposure to carbon nanotubes (Muller et al., 2005; Shvedova et al., 2005; Lam et al., 2006; Porter et al., 2010; Poulsen et al., 2015; Mercer et al., 2011; He et al., 2011). Previous studies laid the groundwork of the underlying biological mechanisms of tissue-level changes by gene expression profiling, several of them included the same MWCNT dose (40 μg) and time point (56 days) (Pacurari et al., 2011; Snyder-Talkington et al., 2016a; Snyder-Talkington et al., 2013). Altered mRNA regulation in those studies indicated involvement of numerous immune cell functions as well as pathways to inflammation/fibrosis.

To our knowledge, there is no published data on the changes in blood cell composition upon pharyngeal aspiration of MWCNTs in mice. In the study by Gotz et al., carbon nanoparticles instillation led to a slight blood neutrophilia 24 h post exposure, although no other time points were been studied (Götz et al., 2011). It was important for us to know whether potential cellular responses in the blood abated by the time of sacrifice. Hematological analysis revealed neither a statistically significant increase in inflammatory cells (white blood cells), nor platelet or clotting system dysfunction (Supplementary Table 1). We also used ImmQuant software to infer alterations in immune cell subsets based on the transcriptional profiles and saw no significant changes in the blood (Supplementary Fig. 3). Lungs, on the other hand, exhibited extensive shifts in immune cell types and activation states: the changes in transcriptional landscape were predicted to be associated with a significant increase in activated macrophages, incoming monocytes, classical monocytes, mature T-cells, and a relative decrease in immature/naïve T-cells (Supplementary Fig. 2). In our previous study we saw similar changes in lungs and bronchoalveolar lavage fluid of mice exposed to MWCNT at the same dose (Khaliullin et al., 2015). This is likely due to the major barrier defense role of the respiratory system, and predefined immune system surveillance/response algorithms.

The overall pattern of gene expression in the mouse lungs 56 days post-exposure showed signs of unresolved inflammation and connective tissue organization. Residual acute phase response was indicated by a 3.6-fold increased *Saa3* expression, while *Saa2* was downregulated 2.3-fold. This exact type of acute phase response pattern has been previously shown to be associated with the exposure to MWCNT in mice (Poulsen et al., 2017). The evidence for chronic inflammatory conditions and adaptive immune responses in the lungs comes from the fact that among the most upregulated genes were Immunoglobulin heavy chains (upregulated 8–12-fold), *Mmp12*, *Spp1* (upregulated 8-fold), *Ptgs1* (upregulated 3.3-fold) and *Timp1* (upregulated 2.7-fold). Four small heat shock proteins (*Hspb1*, *Hspb2*, *Hspb6*, *Hspb7*) were ovexpressed, which are commonly upregulated in response to cellular stress. Upregulation of transcription factors specifically involved in MWCNT lung fibrosis (*Arid5a*, *Mafb*, *Irf7*) was also confirmed by other studies (Zhernovkov et al., 2018). Several prostanoid synthesis-related genes were upregulated in the lungs, which have been previously shown to accompany bleomycin injury and MWCNT exposure (Lee et al., 2012). Moreover, Mitchell et al. proposed a systemic immunosuppression model for MWCNT exposure scenario, wherein TGF-β secreted by lung macrophages causes increased PgE_2 and IL-10 secretion in the spleen, which in turn affects the T-cells (Mitchell et al., 2009).

Myeloid-derived suppressor cells are also recruited to and expanded through the induction/production of COX-2 and PgE_2 (Srivastava et al., 2012). Of special interest was the downregulation of several genes encoding proteins involved in innate immune responses in the lungs, such as *Bpifa* (formerly *Plunc*, 44-fold), *Bpifb1*, *Reg3g*. Increased susceptibility to infectious diseases and immunosuppression have already been shown as one of the characteristic effects of CNT exposure in mice and suspected to modulate immune responses in humans (Shvedova et al., 2008b; Chen et al., 2017; Walling and Lau, 2014). Upregulation of *Cd14* and *Hla-dqa1* in the lungs may reflect the higher activation state of the professional phagocytes. Downregulation of *Rora* (important for the T_H17 effector functions) by MWCNT was observed in vitro and in vivo (Snyder-Talkington et al., 2015; Moraes et al., 2013).

The number of dysregulated genes in the whole blood samples was 15 times lower than in the lung tissue. Possible ER stress induction in the blood cells was indicated by the upregulation of *Rnf183* (Wu et al., 2018). Increased *Vdr* (Vitamin D receptor) expression could be due to its multifactor activity in the immune system (van Etten and Mathieu, 2005): it is upregulated during early stages of immune cell development in mice, thus suggesting increased amounts of younger nucleated immune cells (Janik et al., 2017). Decreased *St 3 gal1* expression may signal perturbations in CD8 T-lymphocytes homeostasis (Priatel et al., 2000). One of the major upregulated genes in whole blood was *Ptger2*, encoding Prostaglandin E_2 receptor 2 (EP_2). This receptor is commonly expressed on naïve CD4 T-lymphocytes and is routinely increased during activation. Signaling through EP_2 also promotes the T_H17 cell development (Boniface et al., 2009). Among the other noteworthy genes, two stand out as involved in DNA repair mechanisms: *Mbd4*, crucial for base excision repair and *Msh2*, responsible for DNA mismatch repair were downregulated in the dataset; these two share a special relationship with *Mbd4* deficiency promoting further *Msh2* decrease (Cortellino et al., 2003). It is vital to note here that without supporting experimental data one should cautiously speculate on the consequences of the altered expression profiles.

Considering the tight homeostatic control of the blood constituents, we were expecting a lower number of dysregulated genes overall. A number of overlapping up-regulated genes between whole blood and lungs are important for the immune function, namely *Cxcr1*, a chemokine receptor, that plays a major role in inflammation, IL-8 signaling, chemotaxis of neutrophils, and cancer (Ha et al., 2017); *Cd72* – a negative regulator of B-cell activation (Parnes and Pan, 2000; Tsubata, 2012), *Sharpin* – an important regulator of inflammatory responses via integrin signaling and NF-kB (Wang et al., 2012a; Wang et al., 2012b), and *Slc11a1* – a metal antiporter, localized in the membranes of late endosomes and lysosomes in macrophages that is implicated in resistance to infections (Blackwell et al., 2001). The solute carrier (SLC) family of proteins includes > 400 members, some of them critical for immune system functions. The recent study by Snyder-Talkington revealed the upregulation of *Slc7a1* and *Slc22a5* not only in the mouse blood and lungs, but also in the human epithelial cells (Snyder-Talkington et al., 2019). It might be prudent to look deeper into the use of SLCs as candidate biomarkers. *Trim24*, down-regulated in both subsets, has been shown to be important for T_H2 cell effector function (Perez-Lloret et al., 2016) and acts as an IFN/STAT pathway suppressor (Tisserand et al., 2011), while also participating in lung cancer progression (Li et al., 2012). Genes commonly involved in mast cell functions were

downregulated in both lungs (*Mmcp-11*) and blood (*Mcpt-8*). Considering that all blood circulates through the lungs, one may expect similar changes in nucleated blood cells to be present in lung tissue (Liew et al., 2006); however, our study reveals many instances of opposing dysregulation patterns between the two tissues. For example, among the genes upregulated in the lungs and downregulated in the blood were *Hla-dqa1* (MHC-II), essential for antigen presentation, and *Lilrb4*, which controls the immune response, limiting reactivity (Cella et al., 1997).

Despite individual genes within big datasets having patterns of dysregulation, novel analysis methods, such as Ingenuity Pathway Analysis, allow for the identification of broader pathologies that may direct further biomarker discovery. Using this technique, we identified canonical pathways, associated biological processes, and functions that aligned with previous description of MWCNT-induced lesion studies (Table 2). Significant involvement of upstream regulators, such as MYD88 and IL-4, is characteristic of concurring inflammation. Upregulated pathways included NFAT activation, which propagates T-cell mediated activities (Masuda et al., 1998). Prominent cell-based immune response was revealed using the regulatory network construction function (Supplementary fig. 4). Comparing the data from Snyder-Talkington et al. (Snyder-Talkington et al., 2013) for 56 days' time point and 40 μg of MWCNT per mouse administered dose, there was a strong overlap between some canonical pathways known to be involved in fibrotic and inflammatory responses, yet several differences have been observed such as FcyR-mediated phagocytosis and calcium signaling. The dissimilarities in responses most likely originate from experimental design variability and differences in the type of MWCNTs utilized.

The fact that cancer, listed as one of the major relevant diseases by IPA in both lungs and blood samples, has opposite activation status between the two datasets, is a major finding of this study. The negative z-score for “cancer” in lungs coincides with the 1.6-fold upregulation of *Trp53*, encoding TP53, which was also predicted to be activated in the “upstream regulators” IPA function along with RB1 tumor suppressor. We have not observed the activation of cancer disorders/pathways in the Snyder-Talkington lung gene expression data (Snyder-Talkington et al., 2013). Contrary to our findings, Pacurari et al. found increases in cancer-related outcomes in their MWCNT-induced lung toxicity study (Pacurari et al., 2011); however, the authors have acknowledged that their results are somewhat biased, because they only analyzed carcinogenesis-related genes (Pacurari et al., 2011). Our genome-wide study might allow for broader biomarker discovery. In the blood, upregulation of cancer/tumor development pathways is in line with the downregulation of *Rb1* and predicted inhibition of TP53 (Supplementary Fig. 7) and KMT2D regulatory molecules, despite no dysregulation of the respective *Trp53* and *Kmt2d* having been observed. KMT2D plays a major role in development and acts as a tumor suppressor in adult tissues (Froimchuk et al., 2017), specifically in B-lymphocytes (Zhang et al., 2015; Ortega-Molina et al., 2015), but also in epithelial cells (Lin-Shiao et al., 2018). The increase in cancer-related mRNAs in the blood following MWCNT exposure was observed by Snyder-Talkington as well (Snyder-Talkington et al., 2016b), but that study used a cancer-prone mouse strain and tumor inducer methylcholanthrene. The disparity in “cancer”-related pathways between the two datasets may lay in the complexity of local inflammatory milieu of lungs versus the subtle humoral and cellular alterations in the whole blood. Nevertheless,

in our opinion, it is plausible to associate this disparity with the opposing predicted TP53 activation status. It should be noted that the IPA accounted for > 500 cancer-related molecules in the lung dataset but only 45 in the blood.

Another significant finding is the common “Hypersensitivity” disorder between the two datasets. T_H2-like inflammation is something previously reported for MWCNT exposures and has been reviewed extensively somewhere else (Dong and Ma, 2018). Aiming for that particular category of disorders could be a viable strategy for the search of biomarkers of exposure to MWCNT.

Future directions include investigating the RNA subtypes: exosomal, non-coding, and mitochondrial RNA species. Another route is to compare animal models and data from humans, yet human exposure to MWCNT is difficult to estimate with reasonable certainty in terms of dose and length of exposure. Interspecies differences in metabolism and gene expression further confound comparisons of biological responses (Lin et al., 2014), however, more and more studies are looking into mouse and human transcriptomes comparisons for such conditions as lung tumors (Jones et al., 2018), chronic obstructive pulmonary disease (Obeidat et al., 2018), and cystic fibrosis (Montoro et al., 2018). Considering the huge variety of carbonaceous nanomaterials and carbon nanotubes in particular, reliable biomarkers of exposure in the whole blood are unlikely to be material-specific, but rather should reflect the specific responses unique to a group of nanoparticles. Several limitations of the current study should be mentioned: mice received a single bolus dose of the material, which is less physiologically relevant than inhalation, and transcripts of interest have not been validated by PCR, since we have not been looking into specific dysregulation statuses, and rather looked at the whole picture. We used “as produced” non-purified MWCNT samples, including metal catalyst impurities that might contribute to the overall toxicity. Care should be taken when generalizing our conclusions to other carbonaceous fibrous particles, even at the same dose and time point.

5. Conclusions

Fifty-six days after pharyngeal aspiration exposure to MWCNT, histopathology and mRNA microarray analysis revealed inflammatory responses and decreased innate immunity functions in the lungs of exposed animals. Collectively, our data are consistent with previous studies, showing a significant involvement of T- and B-cell mediated immunity in MWCNT pulmonary exposure pathogenesis, lasting inflammation, and deregulation of specific genes/pathways in circulating blood cells. Transcriptome changes occurring in the lungs have not produced an exactly replicable pattern in the whole blood; however, we were able to identify several relevant pathways in the blood transcriptome and commonly dysregulated genes. It was also clearly possible to register the systemic response in the whole blood cells using the IPA analysis of dysregulated genes, featuring cancer-related pathways and hypersensitivity, even though the blood cell differentials were not significantly altered between treatment group and controls. While in our opinion it is too early to recommend particular mRNAs from the whole blood as biomarkers of MWCNT effect in humans, we have added to the necessary framework to narrow down the search.

Supplementary Material

Refer to Web version on PubMed Central for supplementary material.

Acknowledgements

We would like to thank Dr. Jayme Coyle for valuable inputs, and Sherri Friend for the FESEM pictures of MWCNT.

Funding

This work was supported by the Nanotechnology Research Center of the National Institute for Occupational Safety and Health (NIOSH NTRC 939011K), and Russian Ministry of Education, Science and Technology (NRF-2011-35B-E00011).

References

Beard JD, Erdely A, Dahm MM, de Perio MA, Birch ME, Evans DE, et al., 2018 Carbon nanotube and nanofiber exposure and sputum and blood biomarkers of early effect among U.S. Workers. Environ Int. 116, 214–228. [PubMed: 29698898]

Blackwell JM, Goswami T, Evans CA, Sibthorpe D, Papo N, White JK, et al., 2001 SLC11A1 (formerly NRAMP1) and disease resistance. Cell. Microbiol 3 (12), 773–784. [PubMed: 11736990]

Boniface K, Bak-Jensen KS, Li Y, Blumenschein WM, McGeachy MJ, McClanahan TK, et al., 2009 Prostaglandin E2 regulates Th17 cell differentiation and function through cyclic AMP and EP2/EP4 receptor signaling. J. Exp. Med 206 (3), 535–548. [PubMed: 19273625]

Brazma A, Hingamp P, Quackenbush J, Sherlock G, Spellman P, Stoeckert C, et al., 2001 Minimum information about a microarray experiment (MIAME)-toward standards for microarray data. Nat. Genet 29 (4), 365–371. [PubMed: 11726920]

Burczynski ME, Dorner AJ, 2006 Transcriptional profiling of peripheral blood cells in clinical pharmacogenomic studies. Pharmacogenomics. 7 (2), 187–202. [PubMed: 16515398]

Castranova V, Schulte PA, Zumwalde RD, 2013 Occupational nanosafety considerations for carbon nanotubes and carbon nanofibers. Acc. Chem. Res 46 (3), 642–649. [PubMed: 23210709]

Cella M, Döhring C, Samaridis J, Dessing M, Brockhaus M, Lanzavecchia A, et al., 1997 A novel inhibitory receptor (ILT3) expressed on monocytes, macrophages, and dendritic cells involved in antigen processing. J. Exp. Med 185 (10), 1743–1751. [PubMed: 9151699]

Chen H, Zheng X, Nicholas J, Humes ST, Loeb JC, Robinson SE, et al., 2017 Single-walled carbon nanotubes modulate pulmonary immune responses and increase pandemic influenza a virus titers in mice. Virol. J 14 (1), 242. [PubMed: 29273069]

Cortellino S, Turner D, Masciullo V, Schepis F, Albino D, Daniel R, et al., 2003 The base excision repair enzyme MED1 mediates DNA damage response to antitumor drugs and is associated with mismatch repair system integrity. Proc. Natl. Acad. Sci. U. S. A 100 (25), 15071–15076. [PubMed: 14614141]

Dahm MM, Schubauer-Berigan MK, Evans DE, Birch ME, Bertke S, Beard JD, et al., 2018 Exposure assessments for a cross-sectional epidemiologic study of US carbon nanotube and nanofiber workers. Int. J. Hyg. Environ. Health 221 (3), 429–440. [PubMed: 29339022]

Dong J, Ma Q, 2018 Type 2 immune mechanisms in carbon nanotube-induced lung fibrosis. Front. Immunol 9, 1120. [PubMed: 29872441]

Dymacek J, Snyder-Talkington BN, Porter DW, Mercer RR, Wolfarth MG, Castranova V, et al., 2015 mRNA and miRNA regulatory networks reflective of multi-walled carbon nanotube-induced lung inflammatory and fibrotic pathologies in mice. Toxicol. Sci 144 (1), 51–64. [PubMed: 25527334]

Erdely A, Dahm M, Chen BT, Zeidler-Erdely PC, Fernback JE, Birch ME, et al., 2013 Carbon nanotube dosimetry: from workplace exposure assessment to inhalation toxicology. Part Fibre Toxicol. 10 (1), 53. [PubMed: 24144386]

Fatkhutdinova LM, Khaliullin TO, Vasil'yeva OL, Zalyalov RR, Mustafin IG, Kisin ER, et al., 2016a Fibrosis biomarkers in workers exposed to MWCNTs. Toxicol. Appl. Pharmacol 299, 125–131. [PubMed: 26902652]

Fatkhutdinova LM, Khaliullin TO, Zalyalov RR, Tkachev AG, Birch ME, Shvedova AA, 2016b Assessment of airborn multiwalled carbon nanotubes in a manufactoring environment. Nanotechnol Russ. 11 (1), 110–116. [PubMed: 28603597]

Frishberg A, Brodt A, Steuerman Y, Gat-Viks I, 2016 ImmQuant: a user-friendly tool for inferring immune cell-type composition from gene-expression data. Bioinformatics. 32 (24), 3842–3843. [PubMed: 27531105]

Froimchuk E, Jang Y, Ge K, 2017 Histone H3 lysine 4 methyltransferase KMT2D. Gene. 627, 337–342. [PubMed: 28669924]

Ghosh M, Oner D, Poels K, Tabish AM, Vlaanderen J, Pronk A, et al., 2017 Changes in DNA methylation induced by multi-walled carbon nanotube exposure in the workplace. Nanotoxicology. 11 (9–10), 1195–1210. [PubMed: 29191063]

Götz AA, Rozman J, Rödel HG, Fuchs H, Gailus-Durner V, Hrabě de Angelis M, et al., 2011 Comparison of particle-exposure triggered pulmonary and systemic inflammation in mice fed with three different diets. Part Fibre Toxicol. 8 (1), 30. [PubMed: 21951864]

Grosse Y, Loomis D, Guyton KZ, Lauby-Secretan B, El Ghissassi F, Bouvard V, et al., 2014 Carcinogenicity of fluoro-edenite, silicon carbide fibres and whiskers, and carbon nanotubes. Lancet Oncol. 15 (13), 1427–1428. [PubMed: 25499275]

Ha H, Debnath B, Neamati N, 2017 Role of the CXCL8-CXCR1/2 Axis in cancer and inflammatory diseases. Theranostics. 7 (6), 1543–1588. [PubMed: 28529637]

He X, Young SH, Schwegler-Berry D, Chisholm WP, Fernback JE, Ma Q, 2011 Multiwalled carbon nanotubes induce a fibrogenic response by stimulating reactive oxygen species production, activating NF-kappaB signaling, and promoting fibroblast-to-myofibroblast transformation. Chem. Res. Toxicol 24 (12), 2237–2248. [PubMed: 22081859]

Iavicoli I, Leso V, Schulte PA, 2016 Biomarkers of susceptibility: state of the art and implications for occupational exposure to engineered nanomaterials. Toxicol. Appl. Pharmacol 299, 112–124. [PubMed: 26724381]

Janik S, Nowak U, Laszkiewicz A, Satyr A, Majkowski M, Marchwicka A, et al., 2017 Diverse regulation of vitamin D receptor gene expression by 1,25-dihydroxyvitamin D and ATRA in murine and human blood cells at early stages of their differentiation. Int. J. Mol. Sci 18 (6).

Jones RA, Franks SE, Moorehead RA, 2018 Comparative mRNA and miRNA transcriptome analysis of a mouse model of IGFIR-driven lung cancer. PLoS One 13 (11), e0206948. [PubMed: 30412601]

Khaliullin TO, Shvedova AA, Kisin ER, Zalyalov RR, Fatkhutdinova LM, 2015 Evaluation of fibrogenic potential of industrial multi-walled carbon nanotubes in acute aspiration experiment. Bull. Exp. Biol. Med 158 (5), 684–687. [PubMed: 25778660]

Kuijpers E, Pronk A, Kleemann R, Vlaanderen J, Lan Q, Rothman N, et al., 2018 Cardiovascular Effects among Workers Exposed to Multiwalled Carbon Nanotubes. 75 (5). pp. 351–358.

Lam CW, James JT, McCluskey R, Arepalli S, Hunter RL, 2006 A review of carbon nanotube toxicity and assessment of potential occupational and environmental health risks. Crit. Rev. Toxicol 36 (3), 189–217. [PubMed: 16686422]

Lee JK, Sayers BC, Chun KS, Lao HC, Shipley-Phillips JK, Bonner JC, et al., 2012 Multi-walled carbon nanotubes induce COX-2 and iNOS expression via MAP kinase-dependent and -independent mechanisms in mouse RAW264.7 macrophages. Part Fibre Toxicol. 9, 14. [PubMed: 22571318]

Li W, 2012 Volcano plots in analyzing differential expressions with mRNA microarrays. J. Bioinforma. Comput. Biol 10 (6), 1231003.

Li H, Sun L, Tang Z, Fu L, Xu Y, Li Z, et al., 2012 Overexpression of TRIM24 correlates with tumor progression in non-small cell lung cancer. PLoS One 7 (5), e37657. [PubMed: 22666376]

Liew CC, Ma J, Tang HC, Zheng R, Dempsey AA, 2006 The peripheral blood transcriptome dynamically reflects system wide biology: a potential diagnostic tool. J. Lab. Clin. Med 147 (3), 126–132. [PubMed: 16503242]

Lin S, Lin Y, Nery JR, Urich MA, Breschi A, Davis CA, et al., 2014 Comparison of the transcriptional landscapes between human and mouse tissues. Proc. Natl. Acad. Sci. U. S. A 111 (48), 17224–17229. [PubMed: 25413365]

Lin-Shiao E, Lan Y, Coradin M, Anderson A, Donahue G, Simpson CL, et al., 2018 KMT2D regulates p63 target enhancers to coordinate epithelial homeostasis. Genes Dev. 32 (2), 181–193. [PubMed: 29440247]

Masuda ES, Imamura R, Amasaki Y, Arai K, Arai N, 1998 Signalling into the T-cell nucleus: NFAT regulation. Cell. Signal 10 (9), 599–611. [PubMed: 9794241]

Mercer RR, Hubbs AF, Scabilloni JF, Wang L, Battelli LA, Friend S, et al., 2011 Pulmonary fibrotic response to aspiration of multi-walled carbon nanotubes. Part Fibre Toxicol. 8, 21. [PubMed: 21781304]

Mercer RR, Scabilloni JF, Hubbs AF, Battelli LA, McKinney W, Friend S, et al., 2013 Distribution and fibrotic response following inhalation exposure to multi-walled carbon nanotubes. Part Fibre Toxicol. 10, 33. [PubMed: 23895460]

Mitchell LA, Lauer FT, Burchiel SW, McDonald JD, 2009 Mechanisms for how inhaled multiwalled carbon nanotubes suppress systemic immune function in mice. Nat. Nanotechnol 4 (7), 451–456. [PubMed: 19581899]

Mohr S, Liew CC, 2007 The peripheral-blood transcriptome: new insights into disease and risk assessment. Trends Mol. Med 13 (10), 422–432. [PubMed: 17919976]

Montoro DT, Haber AL, Biton M, Vinarsky V, Lin B, Birket SE, et al., 2018 A revised airway epithelial hierarchy includes CFTR-expressing ionocytes. Nature. 560 (7718), 319–324. [PubMed: 30069044]

Moraes AS, Paula RF, Pradella F, Santos MP, Oliveira EC, von Glehn F, et al., 2013 The suppressive effect of IL-27 on encephalitogenic Th17 cells induced by multiwalled carbon nanotubes reduces the severity of experimental autoimmune encephalomyelitis. CNS Neurosci Ther. 19 (9), 682–687. [PubMed: 23731464]

Muller J, Huaux F, Moreau N, Misson P, Heilier JF, Delos M, et al., 2005 Respiratory toxicity of multi-wall carbon nanotubes. Toxicol. Appl. Pharmacol 207 (3), 221–231. [PubMed: 16129115]

Nel AE, Parak WJ, Chan WCW, Xia T, Hersam MC, Brinker CJ, et al., 2015 Where are we heading in nanotechnology environmental health and safety and materials characterization? ACS Nano 9 (6), 5627–5630. [PubMed: 26100220]

Obeidat M, Dvorkin-Gheva A, Li X, Bosse Y, Brandsma CA, Nickle DC, et al., 2018 The overlap of lung tissue Transcriptome of smoke exposed mice with human smoking and COPD. Sci. Rep 8 (1), 11881. [PubMed: 30089872]

Ortega-Molina A, Boss IW, Canela A, Pan H, Jiang Y, Zhao C, et al., 2015 The histone lysine methyltransferase KMT2D sustains a gene expression program that represses B cell lymphoma development. Nat. Med 21 (10), 1199–1208. [PubMed: 26366710]

Pacurari M, Qian Y, Porter DW, Wolfarth M, Wan Y, Luo D, et al., 2011 Multi-walled carbon nanotube-induced gene expression in the mouse lung: association with lung pathology. Toxicol. Appl. Pharmacol 255 (1), 18–31. [PubMed: 21624382]

Parnes JR, Pan C, 2000 CD72, a negative regulator of B-cell responsiveness. Immunol. Rev 176, 75–85. [PubMed: 11043769]

Perez-Lloret J, Okoye IS, Guidi R, Kannan Y, Coomes SM, Czieso S, et al., 2016 T-cell–intrinsic Tif1α/Trim24 regulates IL-1R expression on T(H)2 cells and T(H)2 cell-mediated airway allergy. Proc. Natl. Acad. Sci. U. S. A 113 (5) E568–E76. [PubMed: 26787865]

Petrov PD, Bonet ML, Reynés B, Oliver P, Palou A, Ribot J, 2016 Whole blood RNA as a source of transcript-based nutrition- and metabolic health-related biomarkers. PLoS One 11 (5).

Porter DW, Hubbs AF, Mercer RR, Wu N, Wolfarth MG, Sriram K, et al., 2010 Mouse pulmonary dose- and time course-responses induced by exposure to multi-walled carbon nanotubes. Toxicology. 269 (2–3), 136–147. [PubMed: 19857541]

Poulsen SS, Saber AT, Williams A, Andersen O, Kobler C, Atluri R, et al., 2015 MWCNTs of different physicochemical properties cause similar inflammatory responses, but differences in transcriptional and histological markers of fibrosis in mouse lungs. Toxicol. Appl. Pharmacol 284 (1), 16–32. [PubMed: 25554681]

Poulsen SS, Knudsen KB, Jackson P, Weydahl IE, Saber AT, Wallin H, et al., 2017 Multi-walled carbon nanotube-physicochemical properties predict the systemic acute phase response following pulmonary exposure in mice. PLoS One 12 (4), e0174167. [PubMed: 28380028]

Priatel JJ, Chui D, Hiraoka N, Simmons CJ, Richardson KB, Page DM, et al., 2000 The ST3Gal-I sialyltransferase controls CD8+ T lymphocyte homeostasis by modulating O-glycan biosynthesis. Immunity. 12 (3), 273–283. [PubMed: 10755614]

Schubauer-Berigan MK, Dahm MM, Erdely A, Beard JD, Eileen Birch M, Evans DE, et al., 2018 Association of pulmonary, cardiovascular, and hematologic metrics with carbon nanotube and nanofiber exposure among U.S. workers: a cross-sectional study. Part Fibre Toxicol. 15 (1), 22. [PubMed: 29769147]

Schulte P, Leso V, Niang M, Iavicoli I, 2018 Biological monitoring of workers exposed to engineered nanomaterials. Toxicol. Lett 298, 112–124. [PubMed: 29920308]

Shvedova AA, Kisin ER, Mercer R, Murray AR, Johnson VJ, Potapovich AI, et al., 2005 Unusual inflammatory and fibrogenic pulmonary responses to single-walled carbon nanotubes in mice. Am J Physiol Lung Cell Mol Physiol. 289 (5), L698–L708. [PubMed: 15951334]

Shvedova AA, Kisin E, Murray AR, Johnson VJ, Gorelik O, Arepalli S, et al., 2008a Inhalation vs. aspiration of single-walled carbon nanotubes in C57BL/6 mice: inflammation, fibrosis, oxidative stress, and mutagenesis. Am J Physiol Lung Cell Mol Physiol. 295 (4), L552–L565. [PubMed: 18658273]

Shvedova AA, Fabisiak JP, Kisin ER, Murray AR, Roberts JR, Tyurina YY, et al., 2008b Sequential exposure to carbon nanotubes and bacteria enhances pulmonary inflammation and infectivity. Am. J. Respir. Cell Mol. Biol 38 (5), 579–590. [PubMed: 18096873]

Shvedova AA, Yanamala N, Kisin ER, Khailullin TO, Birch ME, Fatkhutdinova LM, 2016a Integrated analysis of dysregulated ncRNA and mRNA expression profiles in humans exposed to carbon nanotubes. PLoS One 11 (3) e0150628–e. [PubMed: 26930275]

Shvedova AA, Yanamala N, Kisin ER, Khailullin TO, Birch ME, Fatkhutdinova LM, 2016b Integrated analysis of dysregulated ncRNA and mRNA expression profiles in humans exposed to carbon nanotubes. PLoS One 11 (3), e0150628. [PubMed: 26930275]

Siegrist KJ, Reynolds SH, Kashon ML, Lowry DT, Dong C, Hubbs AF, et al., 2014, Genotoxicity of multi-walled carbon nanotubes at occupationally relevant doses. Part Fibr Toxicol. 11 (1), 6.

Snyder-Talkington BN, Dymacek J, Porter DW, Wolfarth MG, Mercer RR, Pacurari M, et al., 2013 System-based identification of toxicity pathways associated with multi-walled carbon nanotube-induced pathological responses. Toxicol. Appl. Pharmacol 272 (2), 476–489. [PubMed: 23845593]

Snyder-Talkington BN, Dong C, Zhao X, Dymacek J, Porter DW, Wolfarth MG, et al., 2015 Multi-walled carbon nanotube-induced gene expression in vitro: concordance with in vivo studies. Toxicology. 328, 66–74. [PubMed: 25511174]

Snyder-Talkington BN, Dong C, Porter DW, Ducatman B, Wolfarth MG, Andrew M, et al., 2016a Multiwalled carbon nanotube-induced pulmonary inflammatory and fibrotic responses and genomic changes following aspiration exposure in mice: a 1-year postexposure study. J Toxicol Environ Health A. 79 (8), 352–366. [PubMed: 27092743]

Snyder-Talkington BN, Dong C, Sargent LM, Porter DW, Staska LM, Hubbs AF, et al., 2016b mRNAs and miRNAs in whole blood associated with lung hyperplasia, fibrosis, and bronchiolo-alveolar adenoma and adenocarcinoma after multi-walled carbon nanotube inhalation exposure in mice. J. Appl. Toxicol 36 (1), 161–174. [PubMed: 25926378]

Snyder-Talkington BN, Dong C, Singh S, Raese R, Qian Y, Porter DW, et al., 2019 Multi-walled carbon nanotube-induced gene expression biomarkers for medical and occupational surveillance. Int. J. Mol. Sci 20 (11).

Srivastava MK, Zhu L, Harris-White M, Kar UK, Huang M, Johnson MF, et al., 2012 Myeloid suppressor cell depletion augments antitumor activity in lung cancer. PLoS One 7 (7), e40677. [PubMed: 22815789]

Tisserand J, Khetchoumian K, Thibault C, Dembélé D, Chambon P, Losson R, 2011 Tripartite motif 24 (Trim24/Tif1α) tumor suppressor protein is a novel negative regulator of interferon (IFN)/signal transducers and activators of transcription (STAT) signaling pathway acting through retinoic acid receptor α (Rarα) inhibition. J. Biol. Chem 286 (38), 33369–33379. [PubMed: 21768647]

Tsubata T, 2012 Role of inhibitory BCR co-receptors in immunity. Infect Disord Drug Targets. 12 (3), 181–190. [PubMed: 22394175]

van Etten E, Mathieu C, 2005 Immunoregulation by 1,25-dihydroxyvitamin D3: basic concepts. J. Steroid Biochem. Mol. Biol 97 (1–2), 93–101. [PubMed: 16046118]

Walling BE, Lau GW, 2014 Perturbation of pulmonary immune functions by carbon nanotubes and susceptibility to microbial infection. J. Microbiol 52 (3), 227–234. [PubMed: 24585053]

Wang L, Castranova V, Mishra A, Chen B, Mercer RR, Schwegler-Berry D, et al., 2010 Dispersion of single-walled carbon nanotubes by a natural lung surfactant for pulmonary in vitro and in vivo toxicity studies. Part Fibre Toxicol. 7, 31. [PubMed: 20958985]

Wang Z, Potter CS, Sundberg JP, Hogenesch H, 2012a SHARPIN is a key regulator of immune and inflammatory responses. J. Cell. Mol. Med 16 (10), 2271–2279. [PubMed: 22452937]

Wang Z, Sokolovska A, Seymour R, Sundberg JP, HogenEsch H, 2012b SHARPIN is essential for cytokine production, NF-κB signaling, and induction of Th1 differentiation by dendritic cells. PLoS One 7 (2), e31809. [PubMed: 22348129]

Wang Y, Zhou Y, Graves DT, 2014 FOXO transcription factors: their clinical significance and regulation. Biomed. Res. Int 2014, 925350. [PubMed: 24864265]

Whitney AR, Diehn M, Popper SJ, Alizadeh AA, Boldrick JC, Relman DA, et al., 2003 Individuality and variation in gene expression patterns in human blood. Proc. Natl. Acad. Sci. U. S. A 100 (4), 1896–1901. [PubMed: 12578971]

Winckelmans E, Nawrot TS, Tsamou M, Den Hond E, Baeyens W, Kleinjans J, et al., 2017 Transcriptome-wide analyses indicate mitochondrial responses to particulate air pollution exposure. Environ. Health 16 (1), 87. [PubMed: 28821289]

Wu Y, Li X, Jia J, Zhang Y, Li J, Zhu Z, et al., 2018 Transmembrane E3 ligase RNF183 mediates ER stress-induced apoptosis by degrading Bcl-xL. Proc. Natl. Acad. Sci. U. S. A 115 (12) E2762–E71. [PubMed: 29507230]

Zhang J, Dominguez-Sola D, Hussein S, Lee JE, Holmes AB, Bansal M, et al., 2015 Disruption of KMT2D perturbs germinal center B cell development and promotes lymphomagenesis. Nat. Med 21 (10), 1190–1198. [PubMed: 26366712]

Zhernovkov V, Santra T, Cassidy H, Rukhlenko O, Matallanas D, Krstic A, et al., 2018 Transcriptional regulatory mechanisms of fibrosis development in mouse lung tissue exposed to carbon nanotubes. BioRxiV. 363762.

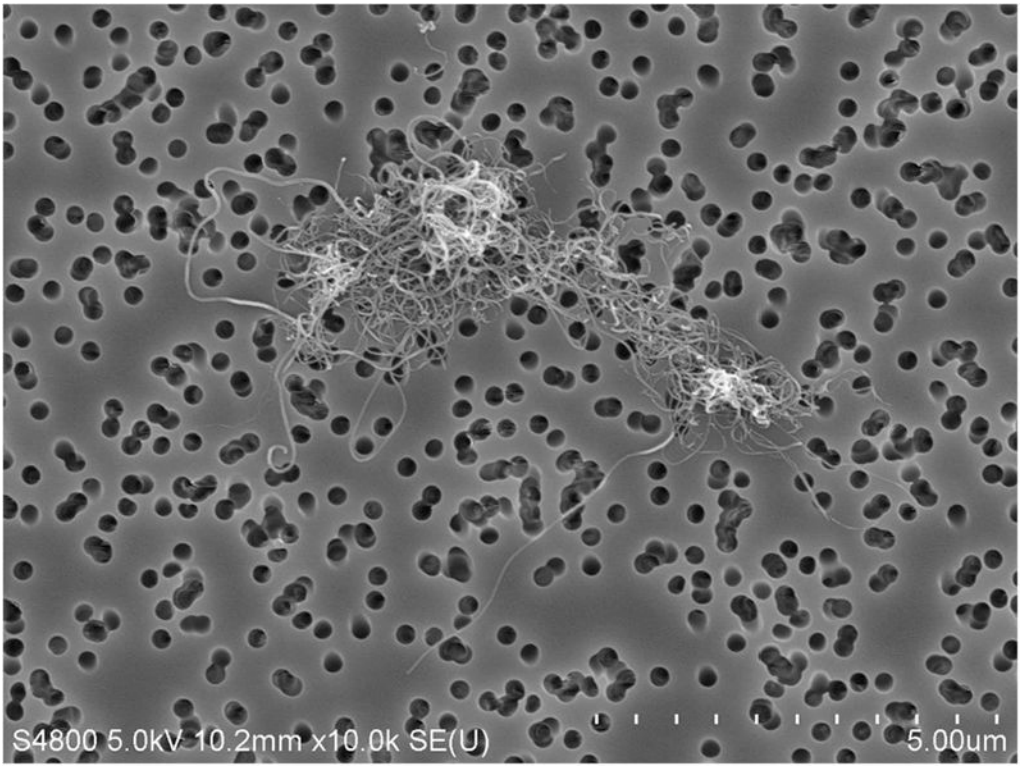

Fig. 1.
Field emission scanning electron microscope photograph of the MWCNT agglomerate from the vehicle solution.

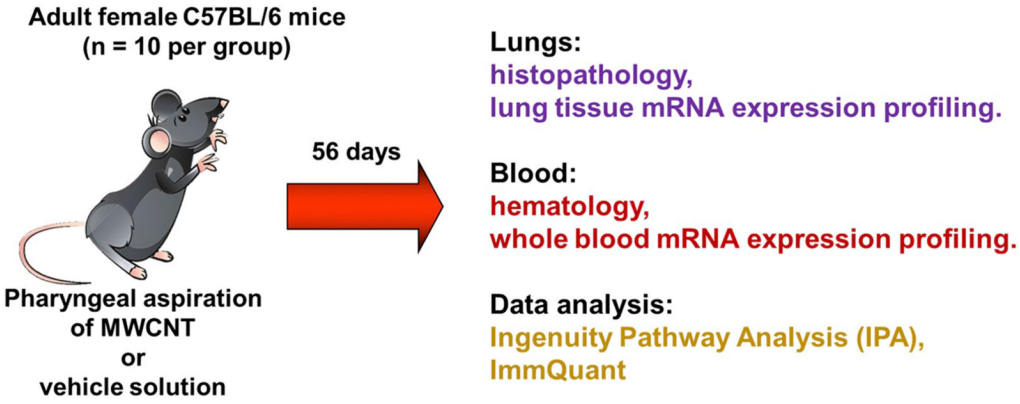

Fig. 2.
Experimental design.

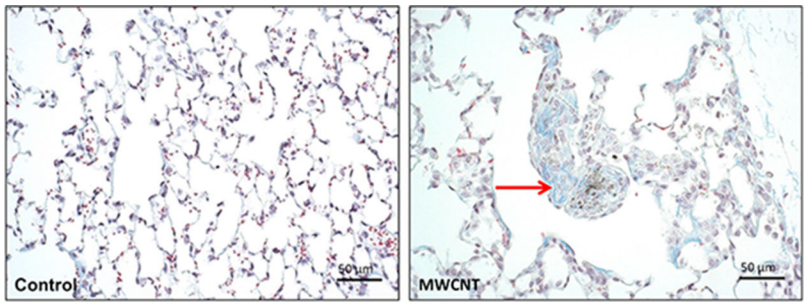

Fig. 3.

Representative histological images of the lung sections of mice exposed to PBS + Survanta® (control) or 40 μg of MWCNT, 56 days post exposure. Arrow points to MWCNT-containing granulomatous lesions with alveolar macrophages and increased collagen deposition (blue coloring). Masson trichrome staining.

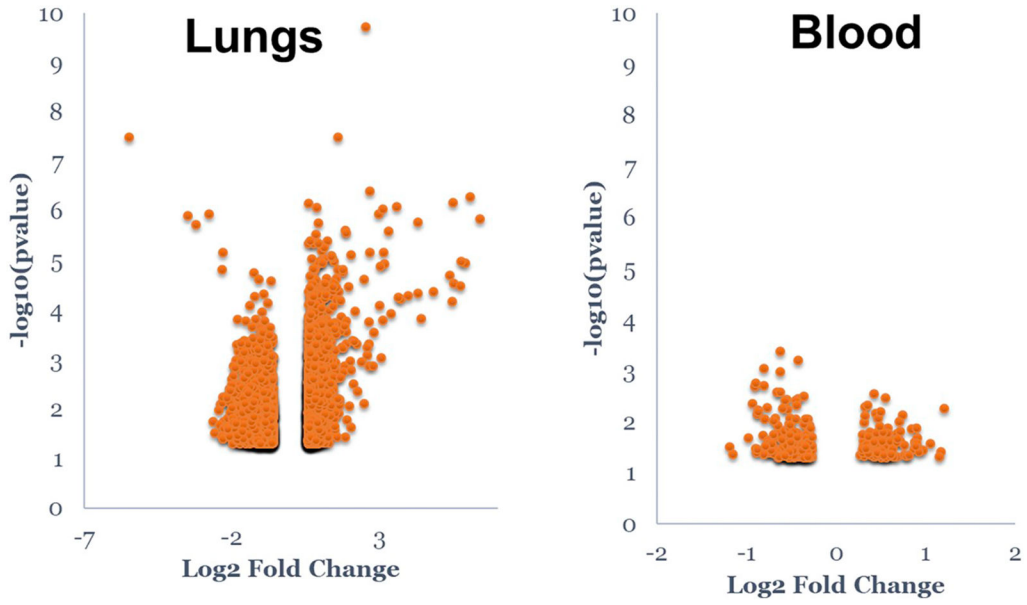

Fig. 4.

Differential gene expression volcano plots. The orange dots in the plots represent differentially expressed genes with statistical significance ($p < 0.05$).

Table 1

Differentially expressed genes, common between two datasets.

Gene name	Expr. FC in the lungs	Expr. FC in the blood
Zbtb7b	1.551	1.226
Tbrg4	1.537	1.228
Sept8	2.554	1.302
Tpp1	1.531	1.345
Cxcr1	6.24	1.358
Dmpk	1.631	1.63
Capg	1.957	1.637
Sharpin	1.55	1.758
Cd72	1.598	1.797
Slc11a1	2.06	1.833
Lpar5	−1.387	−1.766
Arid4b	−1.386	−1.873
Epc1	−1.385	−1.931
Acp1	−1.355	−1.943
Tfeb	−1.343	−2.221
Rpl21	−1.703	−3.695
Spc24	−1.67	−2.182
Otx2	−1.583	−1.836
Trim24	−1.53	−1.964
Cyp4f16/cyp4f37	2.126	−1.906
Leprot	1.578	−1.827
Rapgef6	1.886	−1.653
Glb1	1.567	−1.619
Luc7l2	1.565	−1.599
Gk	1.85	−1.56
Rarg	1.632	−1.482
Zzz3	1.582	−1.479
Auh	1.527	−1.459
Tmf1	1.747	−1.435
Optn	2.53	−1.433
Mbnl1	1.842	−1.425
Rpl12	1.587	−1.4
Hla-dqa1	1.685	−1.381
Lig1	1.858	−1.369
Pla2g12a	1.748	−1.364
Tlk2	1.866	−1.343
Pycr2	1.66	−1.338
Ybx3	1.677	−1.331
Lpin1	1.8	−1.304

Gene name	Expr. FC in the lungs	Expr. FC in the blood
Nfe2	1.88	−1.294
Arid5a	1.636	−1.256
Lilrb4	3.643	−1.243
Ndufa11	1.711	−1.241
Gm10408	−2.533	1.525
NQO2	−2.108	1.866
4930467E23Rik	−1.662	1.895

Table 2

Top diseases and bio functions associated with the dysregulated lung transcriptome (from IPA core analysis).

Top diseases and disorders	**p-value**	**#Molecules**
Inflammatory response	4.23E-03 - 1.34E-09	518
Cancer	4.14E-03 - 2.38E-07	512
Organismal injury and abnormalities	4.30E-03 - 2.38E-07	940
Connective tissue disorders	2.79E-03 - 5.60E-06	148
Inflammatory disease	3.54E-03 - 5.60E-06	184
Top molecular and cellular functions	**p-value**	**#Molecules**
Cell-To-cell signaling and interaction	3.77E-03 - 1.83E-10	333
Cell death and survival	4.30E-03 - 4.65E-09	633
Cellular movement	4.23E-03 - 3.45E-08	391
Protein synthesis	1.94E-03 - 6.63E-08	330
Cellular function and maintenance	4.22E-03 - 1.04E-07	450
System development and function	**p-value**	**#Molecules**
Hematological system dev.	4.30E-03 - 1.83E-10	586
Immune cell trafficking	4.23E-03 - 1.34E-09	314
Organismal survival	1.07E-03 - 1.75E-08	718
Tissue morphology	4.18E-03 - 5.17E-08	614
Humoral immune response	4.30E-03 - 6.63E-08	208

Table 3

Top diseases and bio functions associated with the dysregulated blood transcriptome (from IPA core analysis).

Diseases and disorders	**p-value**	**#Molecules**
Connective tissue disorders	2.74E-02 - 3.55E-04	13
Organismal injury and abnormalities	2.74E-02 - 3.55E-04	75
Skeletal and muscular disorders	2.74E-02 - 3.55E-04	13
Inflammatory response	2.74E-02 - 4.82E-04	26
Cancer	2.74E-02 - 5.74E-04	45
Molecular and cellular functions	**p-value**	**#Molecules**
Cellular assembly and organization	2.74E-02 - 1.89E-04	11
Cell morphology	2.74E-02 - 2.54E-04	38
Cellular development	2.74E-02 - 4.25E-04	36
Cellular growth and proliferation	2.74E-02 - 4.25E-04	35
Small molecule biochemistry	2.74E-02 - 5.63E-04	16
Physiological system development and function	**p-value**	**#Molecules**
Hematological system development and function	2.74E-02 - 8.48E-05	43
Hematopoiesis	2.74E-02 - 8.48E-05	26
Lymphoid tissue structure and development	2.74E-02 - 8.48E-05	35
Organ morphology	2.74E-02 - 8.48E-05	46
Tissue morphology	2.74E-02 - 8.48E-05	58

Toxicol Appl Pharmacol. Author manuscript; available in PMC 2020 December 15.

Table 4

Activation Z-scores of the Diseases and Bio Functions, canonical pathways and upstream regulators, associated with the Dysregulated Transcriptomes. Entries with the Z-score >2 are considered to be activated, while those with Z-score less than −2 are considered to be inhibited.

Diseases and bio functions	**Lung**	**Blood**
Anemia	−2.647	1.492
Hypersensitivity	1.854	1.982
Cancer	−1.741	2.076
Squamous-cell carcinoma	−0.456	1.982
Gastrointestinal tumor	−0.861	1.413
Extracranial solid tumor	−0.506	1.222
Quantity of leukocytes	2.702	−1.222
Quantity of lymphocytes	2.693	−0.744
Quantity of blood cells	2.26	−0.699
Quantity of lymphatic system cells	2.634	0.059
Quantity of lymphoid tissue	1.999	0.015
Quantity of hematopoietic progenitor cells	0.873	0.851
Quantity of phagocytes	0.221	−0.081
Canonical pathways	**Lung**	**Blood**
Protein Kinase A Signaling	−1.109	0.816
Phospholipase C Signaling	2.949	−1.633
Endothelin-1 Signaling	3.015	−1.342
Upstream regulators	**Lung**	**Blood**
TP53	2.879	−2.553
Hbb-b1	4.2	−1.109
GATA1	0.128	−1.969
FOXM1	1.343	0.218